








Cite this: *J. Mater. Chem. A*, 2023, **11**, 3514

## Wearable energy storage with MXene textile supercapacitors for real world use†

Alex Inman,  ‡<sup>a</sup> Tetiana Hryhorchuk,  ‡<sup>a</sup> Lingyi Bi,  <sup>ab</sup> Ruocun (John) Wang,  <sup>a</sup> Ben Greenspan, <sup>c</sup> Taylor Tabb,  <sup>c</sup> Eric M. Gallo, <sup>c</sup> Armin VahidMohammadi, <sup>a</sup> Genevieve Dion, <sup>b</sup> Andreea Danielescu  <sup>\*c</sup> and Yury Gogotsi  <sup>\*a</sup>

Successful implementation of wearable electronics requires practical wearable energy storage systems that can meet certain power and energy metrics. However, flexible, stretchable, and truly textile-grade energy storing platforms have so far remained missing from most e-textile systems due to the insufficient performance metrics of current available materials and technologies. Two-dimensional (2D) transition metal carbides and nitrides (MXenes) offer unique combinations of properties including metallic conductivity, high specific capacitance, hydrophilicity, and solution processability, as well as mechanical flexibility and robustness that render these materials promising for flexible wearable energy storage technologies. Here we demonstrate textile-based electrochemical capacitor devices with a high areal loading of  $\text{Ti}_3\text{C}_2\text{T}_x$  that can be integrated in series *via* a stacked design approach and meet the real-world power requirements for wearable electronics. A demo textile supercapacitor with 5 cells in series, a footprint area of  $25\text{ cm}^2$  and an MXene loading of  $24.2\text{ mg cm}^{-2}$  could operate in a 6 V voltage window delivering an energy density of  $0.401\text{ mW h cm}^{-2}$  at a power density of  $0.248\text{ mW cm}^{-2}$ , and an areal capacitance of  $146\text{ mF cm}^{-2}$  at a  $0.16\text{ mA cm}^{-2}$  discharge current. The MXene textile supercapacitor powers a temperature monitoring system requiring high current densities with wireless data transmission to a receiver for 96 minutes. Power time is a crucial subject for integration of flexible supercapacitors with commercial microelectronics and successful commercialization of smart garments. This initial report of an MXene textile supercapacitor powering a practical peripheral electronics system demonstrates the potential of this family of 2D materials to support a wide range of devices such as motion trackers and biomedical monitors in a flexible textile form factor.

Received 17th November 2022  
Accepted 10th January 2023

DOI: 10.1039/d2ta08995e

rsc.li/materials-a

## Introduction

Smart wearable electronics is a quickly developing area of research.<sup>1–3</sup> A subfield of these wearables, known as electronic textiles or e-textiles, integrates conformable electronics with traditional soft goods.<sup>4–6</sup> E-textiles have relevance across a range of technologies like Internet of Things (IoT), extended reality<sup>7</sup> and especially healthcare, where remote<sup>8</sup> and in-person care<sup>9</sup> can benefit greatly from prolonged wireless monitoring using soft, human-friendly materials.

MXene-based energy storage devices (Fig. 1a) allow for an integrated sensing, processing and communication system powered only by a small textile energy storage unit. Previous studies<sup>10–17</sup> focused primarily on material characterization and were limited in their ability to power a real system consisting of peripheral electronics hardware (Table S1†). Our work focuses on developing a textile-based supercapacitor energy storage device that can meet the real-world power requirements for wearable electronics, enabled by a novel approach in configuring and stacking  $\text{Ti}_3\text{C}_2\text{T}_x$  MXene electrodes on cotton prepared through a drop casting method.

MXenes have a general formula of  $\text{M}_{n+1}\text{X}_n\text{T}_x$  ( $n = 1, 2, 3$  or  $4$ ), where M is an early transition metal, X is carbon or nitrogen, and  $\text{T}_x$  stands for the surface terminations (*e.g.*, OH, O or F). MXenes can be synthesized from a variety of available layered ceramic precursor materials, such as MAX phases,<sup>18</sup> and processed into aqueous dispersions, printing inks, coatings on textile, and pure or composite fibers.<sup>19,20</sup>  $\text{Ti}_3\text{C}_2\text{T}_x$  MXene has negatively charged  $-\text{F}$ ,  $-\text{O}$ , and  $-\text{OH}$  terminated surfaces, resulting in its highly negative zeta potential of below  $-30\text{ mV}$  in water at neutral pH,<sup>21</sup> resulting in stable water dispersion

<sup>a</sup>A.J. Drexel Nanomaterials Institute and Department of Material Science and Engineering, Drexel University, 3141 Chestnut St., Philadelphia 19104, PA, USA. E-mail: gogotsi@drexel.edu

<sup>b</sup>Center for Functional Fabrics, Drexel University, 3141 Chestnut St., Philadelphia 19104, PA, USA

<sup>c</sup>Accenture Labs, 415 Mission St. Fl. 34, San Francisco 94105, CA, USA. E-mail: andreea.danielescu@accenture.com

† Electronic supplementary information (ESI) available. See DOI: <https://doi.org/10.1039/d2ta08995e>

‡ These authors have contributed equally to this work.

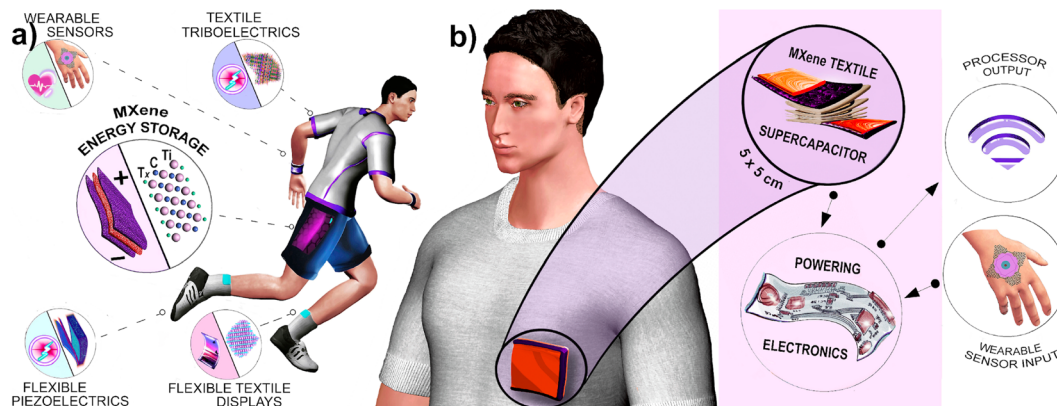


Fig. 1 (a) MXene-based energy storage potential applications (b) required metrics (properties) for integration of a textile supercapacitor, focusing on flexible energy storage and its integration with peripheral electronics, where a  $\text{Ti}_3\text{C}_2\text{T}_x$  MXene textile supercapacitor with a  $5 \times 5 \text{ cm}^2$  footprint powers programmable electronics.

without the need for additives or surfactants.<sup>22</sup> These stable dispersions can be applied *via* dip coating,<sup>23</sup> spray coating<sup>24</sup> and drop casting<sup>25</sup> or other techniques to fibers, yarns and fabrics.  $\text{Ti}_3\text{C}_2\text{T}_x$  is the most studied MXene composition with established and scalable synthesis methods,<sup>20</sup> a high electronic conductivity ( $\sim 20\,000 \text{ S cm}^{-2}$ )<sup>26</sup> and specific capacitances reaching beyond  $400 \text{ F g}^{-1}$  (operating at charging rates of up to  $100 \text{ V s}^{-1}$ ).<sup>27</sup> These properties make  $\text{Ti}_3\text{C}_2\text{T}_x$  a promising electrode candidate for fabrication of textile supercapacitors. Moreover, its solution processability makes  $\text{Ti}_3\text{C}_2\text{T}_x$  compatible with various existing textile-processing techniques in the industry. Previous studies have integrated  $\text{Ti}_3\text{C}_2\text{T}_x$  into fibers and textiles through dip coating,<sup>23</sup> thermal inkjet printing,<sup>22</sup> wet spinning,<sup>28</sup> and electrospinning.<sup>29</sup> Some studies reported sufficient mechanical strength to withstand industrial knitting.<sup>30</sup> However, demonstrated applications only include simple devices such as a wearable wrist band<sup>28</sup> or lighting up LEDs.<sup>22</sup> Despite these considerable efforts in fabrication of MXene fibers and textiles and development of wearable supercapacitors based on them (Table S1†), the majority of the reported data show relatively low energy values, making them impractical for real-world use.

Herein, we use aqueous  $\text{Ti}_3\text{C}_2\text{T}_x$  paints and woven hydrophobic textiles to fabricate supercapacitors for powering real world electronics (Fig. 2). We evaluated two coating approaches: dip coating and drop casting – to find the more efficient way for fabric coating and device fabrication. Moreover, we demonstrate a device prepared by stacking 5 cells in series that can operate in a 6 V voltage window with an energy density of  $0.401 \text{ mW h cm}^{-2}$ , at a power density of  $0.248 \text{ mW cm}^{-2}$  and which is capable of powering a wireless programmable sensor system.

A key consideration in designing textile-based supercapacitors is to maximize the energy storage capability per minimal garment area. This consideration minimizes device footprint and mass of the MXene active material, therefore reducing overall cost, and increases device design flexibility and wearability of the e-garment. To achieve this, we manufactured textile supercapacitors by drop-casting  $\text{Ti}_3\text{C}_2\text{T}_x$  dispersed in water onto cotton fabric and assembling the MXene-infiltrated fabric in a stacked

configuration. We optimized charge/discharge protocols and, as a proof-of-concept, powered peripheral electronic hardware consisting of a modified Arduino Pro Mini, a 2.4 GHz transceiver and a temperature sensor, solely using the fabricated MXene textile supercapacitor. Our demo MXene-based device proves successful prolonged powering of an integrated sensor-processor system, without ultra-low power optimization typical of commercial wearables. In particular, the system demonstrates the ability of an MXene supercapacitor to handle rapidly switching loads, typical of wearable applications where energy saving techniques frequently use standby methods to limit consumption between active periods.

One of the approaches to maximize the performance of the device was using LiCl/PVA gel electrolyte which significantly increases the voltage window while providing a less aggressive environment in opposite to conventional acidic electrolytes such as  $\text{H}_2\text{SO}_4$ ,<sup>25,27</sup>  $\text{H}_3\text{PO}_4$ ,<sup>30</sup> *etc.* which in opposite to LiCl/PVA are known to provide higher capacitance but a lower voltage when used when coupled with active MXene material. It is also worth noting that acidic electrolytes are less desired for textile devices, as they are more likely to corrode wiring or cause skin irritation if the sealing is damaged during use.

## Experimental

More detailed experimental protocols are available within the ESI.†

### MAX and $\text{Ti}_3\text{C}_2\text{T}_x$ MXene synthesis

The Al- $\text{Ti}_3\text{AlC}_2$  MAX powder (MAX phase high stoichiometry ratio of Ti : C) was produced through the high-aluminum content protocol as developed by Mathis *et al.*<sup>26</sup> For  $\text{Ti}_3\text{C}_2\text{T}_x$  MXene synthesis, the mixed HF/HCl acid etching solution protocol was applied.<sup>31–33</sup>

### $\text{Ti}_3\text{C}_2\text{T}_x$ MXene flake size selection

It was shown previously<sup>34</sup> that the size distribution of MXene affects its electrochemical performance. A  $\text{Ti}_3\text{C}_2\text{T}_x$  MXene

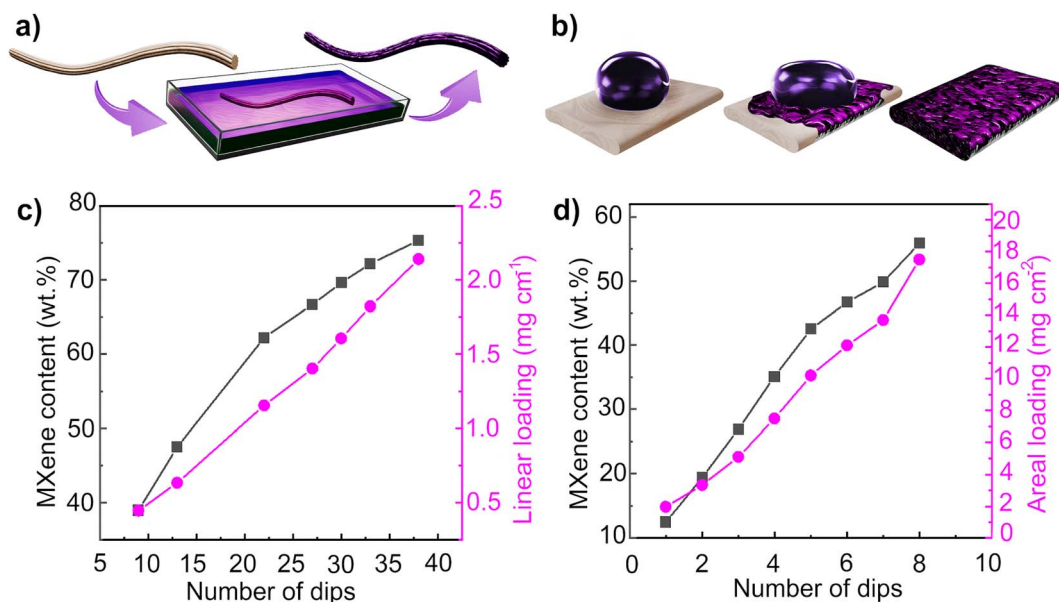


Fig. 2  $\text{Ti}_3\text{C}_2\text{T}_x$  coating of (a) yarns and (b) fabrics. (c) Mass loading of  $\text{Ti}_3\text{C}_2\text{T}_x$  in dips of approximately 390 nm, 15 mg mL<sup>-1</sup> aqueous  $\text{Ti}_3\text{C}_2\text{T}_x$  solution for yarn coating and (d) mass loading of  $\text{Ti}_3\text{C}_2\text{T}_x$  in drop casting cycles of approximately 530 nm, 14 mg mL<sup>-1</sup> aqueous  $\text{Ti}_3\text{C}_2\text{T}_x$  solution for fabric coating.

dispersion in DI water was probe sonicated using a sonic dismembrator, Fisherbrand Model 503, applying an 'on' pulse time of 8 s, 'off' pulse time of 2 s; vibration amplitude 20%. The dispersion concentrations and flake sizes were of comparable

values: approximately 15 mg mL<sup>-1</sup> and approximately 390 nm for yarn dip coating; approximately 14.0 mg mL<sup>-1</sup> and approximately 530 nm for fabric drop casting (Fig. S1†).

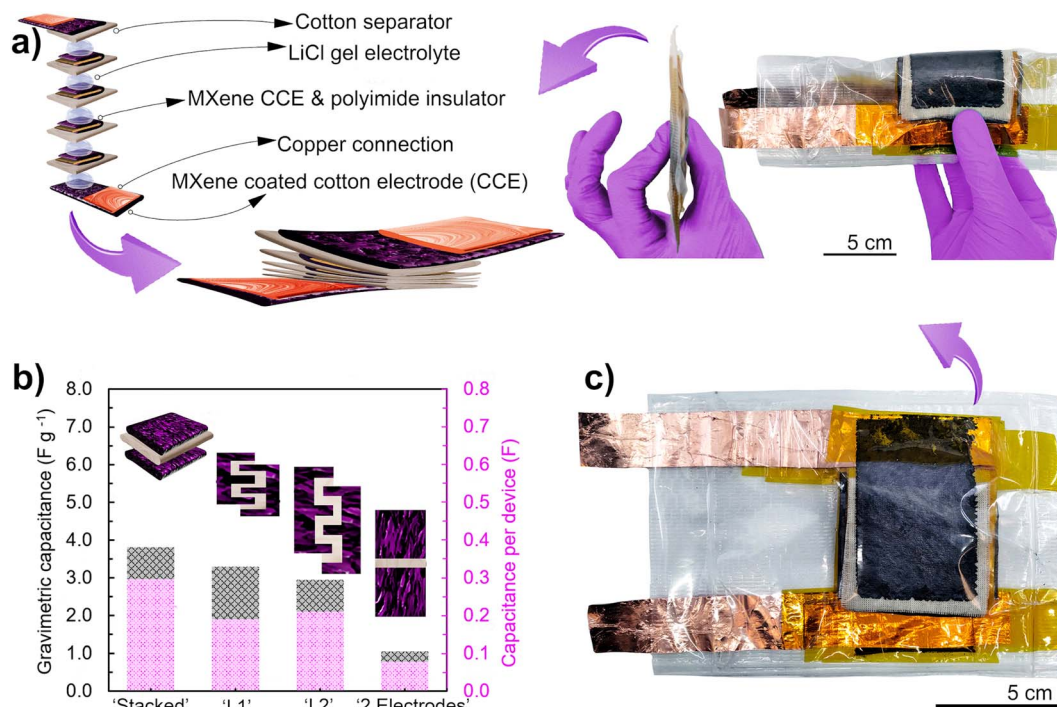


Fig. 3 (a) Schematic and image of a 6 V 'stacked' supercapacitor, packaged in a vacuum sealed bag. (b) Comparing the gravimetric capacitance and total capacitance per device vs. supercapacitor geometry configurations. The geometry configurations are as follows: 'Stacked', '1.1' interdigitated 1, '1.2' interdigitated 2 and '2.Electrodes'. The 'stacked' configuration is most efficient from the material's standpoint (gravimetric capacitance values) and from the device design standpoint (capacitance per device values). (c) Additionally, a 'stacked' supercapacitor is thin and easy to bend.

### Gel electrolyte preparation

20.4 g anhydrous LiCl (lithium chloride, anhydrous, 99%, –20 mesh, purchased from Alfa Aesar) was mixed manually with 60 mL DI water, and thereafter mixed with 6 g of PVA powder (poly(vinyl alcohol) Mw 85 000–124,000, 99+% hydrolyzed linear formula:  $[-CH_2CHOH-]_n$ , purchased from Sigma-Aldrich) at 80 °C and 400 rpm for 6 h.

### Supercapacitor device fabrication

Electrode preparation is described in detail within the ESI.† The assembly of the device was carried out as follows. The bottom electrode was placed underneath a flat surface. Electrolyte was added on top of the electrode to cover the footprint area. A porous cotton separator was placed on top to prevent the electrode from shorting while allowing ions in the electrolyte to pass freely from one electrode to the other. Next, a portion of the

electrolyte was added on top of the cotton separator. In such a manner, cotton, acting as a porous separator, was soaked with LiCl/PVA gel electrolyte. Since the electrolyte was added on both the top and bottom of the cotton separator there was approximately 20  $\mu$ L of electrolyte soaked per each square centimeter of porous cotton separator lying within the footprint area of the device. It is important to control the amount of electrolyte measured by the micropipette (Fisherbrand™ Elite™ Adjustable-Volume Pipette) in order to prevent the leakage of electrolyte which will cause electrical shortage. The first banded electrode pair was placed on top of the electrolyte layer. The next layer of electrolyte was added on the top electrode located from the opposite side of the Kapton (polyimide) insulator layer, and a cotton separator was placed thereafter until five pairs of electrodes were stacked in series. At the end, the stacked configuration was obtained with ten electrodes forming five

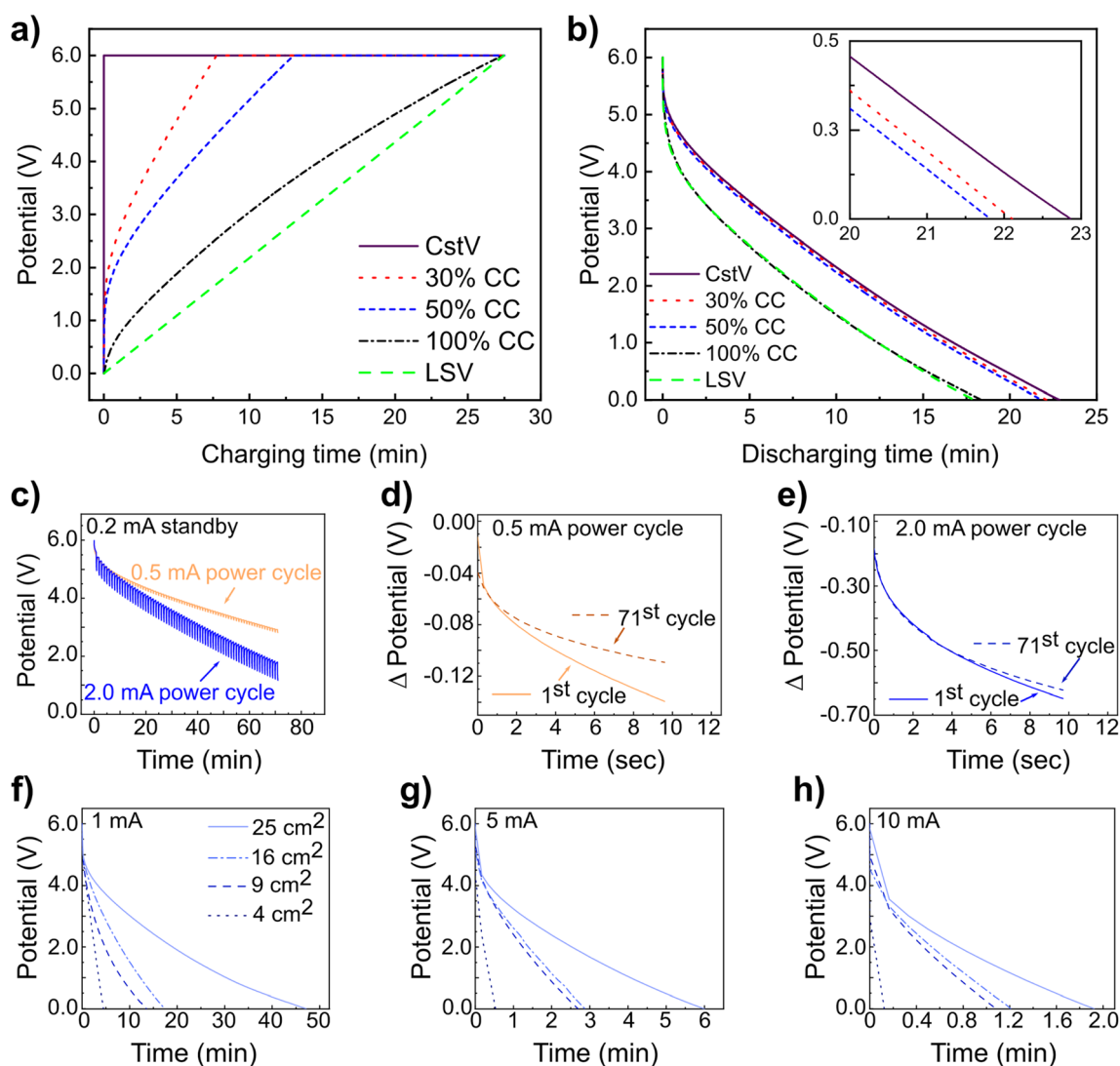


Fig. 4 (a) Different charging protocols for a textile-based supercapacitor and (b) the resulting discharge profiles. The discharge profile of the device with alternating currents for (c) standby and power mode charged with LSV for 30 minutes, and analysis of single power cycles of (d) 0.5 mA and (e) 2.0 mA. Galvanostatic cycling with potential limitation aka constant current (CC) analysis of sandwich design 6 V cells with different areas at (f) 1.0 mA, (g) 5 mA and (h) 10 mA.



cells connected in series. The topmost and bottommost electrodes were attached to copper tabs and the whole device was vacuum sealed. The same procedure (described above) was used for preparation of all devices. There were four devices prepared with footprint areas of 4 cm<sup>2</sup>, 9 cm<sup>2</sup>, 16 cm<sup>2</sup> and 25 cm<sup>2</sup> (MXene loading was as follows: 3.9 mg cm<sup>-2</sup>, 3.5 mg cm<sup>-2</sup>, 2.8 mg cm<sup>-2</sup>, and 5.3 mg cm<sup>-2</sup> respectively (Tables S2 and S3†)). The volume of LiCl gel electrolyte per device was 0.4 mL, 0.9 mL, 1.6 mL and 2.5 mL, respectively. Each device contained 10 electrodes stacked on top of each other in a five cell series configuration. Additionally, flat device configurations with multiple electrodes were explored (Fig. S2†). However, the stacked configuration showed more promise from an application standpoint (Fig. S3†).

### Electrochemical characterization

The charging methods shown in Fig. 4a are denoted as follows: CV (constant voltage), 10% CC (constant current), 30% CC, 50% CC, 100% CC and LSV (linear sweep voltammetry). In the CV charging tests, the sample was immediately brought to 6 V. The percentage CC tests are the percentage of time the device spent charging at CC to reach 6 V, and the remainder of the time was under CV conditions at 6 V. To calculate the current necessary to reach 6 V in the allotted time, a calibration curve was generated, and the sample was charged with the calculated currents (Fig. S4†). LSV ramped the voltage up linearly from 0 V to 6 V over 27.5 min.

## Results and discussion

In the fabricated textile devices, binder-free and additive-free Ti<sub>3</sub>C<sub>2</sub>T<sub>x</sub> MXene acts as the active material in both the positive and negative electrodes. MXene electrodes do not require metal current collectors. Hydrophobic woven cotton textile is used as the substrate and separator (Fig. S5†), and LiCl/PVA gel is used as the electrolyte. For the device design, we integrated cells in series *via* a stacked architecture. This allows us to accommodate the voltage requirements for peripheral hardware. The device voltage linearly increases (based on eqn (1)) by increasing the number of cell stacks within the device in a serial architecture while the overall specific capacitance decreases according to eqn (2). However, since stored energy is proportional to the square of the operating voltage (eqn (3)), such an architecture results in an overall increase in the energy density of the device.

$$V_{\text{series}} = \sum_i V_i \quad (1)$$

$$\frac{1}{C_{\text{series}}} = \frac{1}{C_1} + \frac{1}{C_2} + \dots + \frac{1}{C_n} \quad (2)$$

$$E = \frac{1}{2} C_{\text{series}} V_{\text{series}}^2 \quad (3)$$

Our final device combined five cells in series to achieve a voltage window of 6 V, and an electrode area of 25 cm<sup>2</sup>. To limit the space taken up by the device on the garment for

practical use, the cells were stacked one on top of another to achieve a footprint area matching the electrode area of 25 cm<sup>2</sup>. To test the device design, we compared and determined the optimal charging protocol and measured the effects of variable current discharge and electrode area on performance. Finally, the device is integrated with a voltage regulator to power peripheral hardware, demonstrating its practical use for wearable electronics.

### Material design: MXenes and textile

The standard physical characteristics of Ti<sub>3</sub>C<sub>2</sub>T<sub>x</sub> MXenes are shown in Fig. S1 and Table S4.† The synthesized Ti<sub>3</sub>C<sub>2</sub>T<sub>x</sub> materials showed an electronic conductivity of ~9210 S cm<sup>-2</sup> and hydrophilic properties, making them ideal building blocks for textile-based supercapacitors and real-world flexible electronics. Due to the high vapor pressure of water, the coated substrates can be air dried under ambient conditions. To achieve the desired loading, deposition can be repeated as many times as necessary. Increasing the Ti<sub>3</sub>C<sub>2</sub>T<sub>x</sub> MXene loading leads to higher conductivity of the coated fibers and fabrics and enhanced capacitance of the textile supercapacitors.<sup>23</sup> Cellulosic fibers, yarns, and fabrics (*e.g.*, cotton, linen, and bamboo) are good substrates for MXene coating as the fibrous structure supplies a large surface area for MXenes to adhere to. As shown in Fig. 2 cotton yarn (Nile Organic Cotton from Silk City Fibers) and woven muslin cotton (Mybecca 100% Natural Cotton Muslin Woven Fabric Unbleached) were used as substrates. Ti<sub>3</sub>C<sub>2</sub>T<sub>x</sub> MXene with a small flake size (approximately 530 nm) was used in this study because it was shown to minimize the loss of MXene from fabric since smaller flakes cover individual fibers more efficiently and adhere stronger to the cellulose.<sup>23</sup> A smaller flake size is also beneficial for fast transport of ions. This work compares two different techniques to coat textiles with Ti<sub>3</sub>C<sub>2</sub>T<sub>x</sub> MXenes, dip coating cotton yarns (Fig. 2a) and drop casting on hydrophobic cellulosic fabrics (Fig. 2b) with Ti<sub>3</sub>C<sub>2</sub>T<sub>x</sub> dispersions consisting of small flakes. Both processes were repeated with air drying between coatings. The effectiveness of the two coating methods is compared in Fig. 2c and d. After 38 rounds of dip coating, the linear loading of MXenes on hydrophilic cotton yarn is 2.14 mg cm<sup>-1</sup> and the mass percent loading of MXene of the yarn is 75.3%. On the other hand, after 8 drop cast cycles the areal loading of MXenes on hydrophobic cotton fabrics (Fig. S5†) was 17.5 mg cm<sup>-2</sup> and the mass percent loading was 55.9%. Since achieving the same loading on the yarn by dip-coating would require about 20 cycles, a higher percent loading of MXenes is achieved per deposition by drop casting than by dip coating. This increase in effectiveness is due to the surface tension of the MXene solution when drop cast onto hydrophobic cotton fabrics, which allows for thicker wet deposition when compared to dip coating, resulting in more MXenes deposited per deposition.<sup>23</sup> Drop casting results in MXenes mostly remaining on the surface of the fabric (Fig. 2b) while dip coating allows MXenes to penetrate deeply into the fabric (Fig. 2a). Therefore, the tested devices were fabricated by drop casting MXene flakes onto hydrophobic cotton. For the coated textile to store enough energy and power peripheral

electronics hardware, an appropriate amount of the  $\text{Ti}_3\text{C}_2\text{T}_x$  MXene should be loaded onto the textile substrate. The minimum loading for tested samples was 3 to 4  $\text{mg cm}^{-2}$ . The maximum resistance for the tested samples was 30  $\Omega$  per 9 cm length of the electrode as tested by using a 2-point probe (Tables S2 and S3†).

### Device design: supercapacitor configuration

To achieve the necessary power and energy requirements for running a microcontroller, we used the stacked supercapacitor design configuration shown in Fig. 3a. Before settling on a stacked design for the final case study, a series of designs were first investigated. As shown in Fig. 3b gravimetric capacitance ( $\text{F g}^{-1}$ ) and total capacitance (F) are compared with respect to  $\text{Ti}_3\text{C}_2\text{T}_x$  supercapacitor configurations. For this comparison, four different designs were tested. The first configuration is a 'stacked' design (Fig. 3a), where two electrodes are stacked on top of each other with a porous cotton fabric separating them. In the second configuration ('2.Electrodes'), we placed two electrodes with the same area of active  $\text{Ti}_3\text{C}_2\text{T}_x$  side by side. The other two configurations are interdigitated designs, one that has the same total electrode area as the stacked design (interdigitated 'I.2') and one that takes up the same footprint area as the stacked design (interdigitated 'I.1'). The two interdigitated designs were chosen as "classic" configurations that minimize ionic resistance and eliminate the need for a separator, when the design is limited to two dimensions.<sup>6</sup> The electrode areas, electrode masses, footprint areas and spacing between the electrodes can be found in Table S5.†

Fig. 3b shows that the single cell stacked design outperforms the other designs in both gravimetric capacitance as well as the total capacitance (Fig. S6†) of the single cell devices. The increase in gravimetric capacitance is assumed to be due to the decreased gap between the electrodes. The decrease in the gap distance is allowed by the stacked design with a porous cotton separator sandwiched between the electrodes as opposed to the large gaps between electrodes in the side-by-side configurations. Moreover, stacked devices can be assembled in series vertically while preserving the footprint of a single cell. When we put cells in series, it extends the voltage of the supercapacitor that is necessary for powering many peripheral electronic hardware systems, including the peripheral hardware we used in this work. The area, which the device would take up on a garment (*i.e.*, the footprint area), was tested using four different devices. Each device had five cells stacked in series, with one device on top of another (Fig. 3a) providing a voltage window of 6 V. Because of the stacked configuration, the cells had electrode areas that were the same as the footprint area: 4  $\text{cm}^2$ , 9  $\text{cm}^2$ , 16  $\text{cm}^2$ , and 25  $\text{cm}^2$  (MXene loading was as follows: 3.9  $\text{mg cm}^{-2}$ , 3.5  $\text{mg cm}^{-2}$ , 2.8  $\text{mg cm}^{-2}$ , and 5.3  $\text{mg cm}^{-2}$ , respectively (Tables S2 and S3†)). The devices were tested using the galvanostatic charge–discharge technique at discharge currents of 1 mA, 5 mA and 10 mA (Fig. 4f–h). The time the devices took to discharge from 6 V to 0 V is proportional to the footprint area and inversely proportional to the withdrawing current. At a given current, the total discharge time of a device

was relative to its area with a 25  $\text{cm}^2$  footprint area (5.3  $\text{mg cm}^{-2}$  MXene loading) performing the best across all the currents, and a 4  $\text{cm}^2$  footprint area performing the worst. Discharge current is inversely proportional to the time for the device to discharge from 0 V to 6 V. The best performance was a discharge time of 47 min 12 s for the 25  $\text{cm}^2$  footprint area (5.3  $\text{mg cm}^{-2}$  MXene loading) device at a discharge current of 1 mA. The performance of the devices was also examined by monitoring the time for which the devices were able to power an Arduino Pro Mini 3.3 V microcontroller (Fig. S3†). No loss in efficiency (as the time for which devices were able to power microcontrollers increased with respect to the increase in footprint area) was observed relative to the electrode area or the mass loading as the devices increased in footprint area (Fig. S7†). This shows scalability of the proposed design. After examining the differences in performance as a function of device design (Fig. 3b) and electrode size (Fig. 4f–h), we decided on a final design that had 25  $\text{cm}^2$  electrodes in a stacked configuration. To accommodate the voltage requirements of the peripheral electronics we stacked 5 cells, one on top of the other, to achieve a maximum of 6 V (Fig. 3a).

The final supercapacitor had a footprint of 25  $\text{cm}^2$  per electrode (MXene loading of 24.2  $\text{mg cm}^{-2}$ ). For device preparation and testing a LiCl/PVA gel electrolyte was used. LiCl electrolytes significantly increase the voltage window for MXene supercapacitors,<sup>35</sup> which is important to achieve higher energy densities in devices for powering peripheral electronics hardware. In contrast, using PVA/ $\text{H}_2\text{SO}_4$  as the electrolyte for the fabricated textile supercapacitors, oxygen evolution reaction peaks and MXene oxidation are observed at potentials higher than 0.5 V (Fig. S8†) limiting the operating voltage window of our devices.

The LiCl/PVA gel electrolyte, however, allows a single cell to reach 1.2 V. The use of gel as the electrolyte is optimal from a packaging point of view for wearables because a higher viscosity means better control of the deposition on the electrode than when using a non-gel electrolyte and a lower probability of leakage and electrolyte loss. Another advantage of the LiCl/PVA electrolyte over other electrolytes (in particular  $\text{H}_2\text{SO}_4$ ) is that LiCl is safer to use next to skin and less aggressive towards the textile substrate.<sup>35,36</sup> It should be noted that the shelf life of the textile supercapacitor is strongly affected by water evaporation. Therefore, we used vacuum sealing as the packaging method to seal the device from the environment. This packaging approach could be applicable to commercial products by laminating polymer layers on both sides of the textile supercapacitor after assembly.

### Charging methodology and electrical characterization

**Variable current discharging.** Rapidly switching current loads are commonly found in low power electronic designs, with the devices operating in short bursts to conserve power but preserve core functionality, like reading a sensor or transmitting data. When not performing a measurement, the system goes into standby, drawing considerably less power. To validate how the MXene textile supercapacitors would handle

a switching load current, simulated testing was performed to evaluate performance as the current switched between a “standby” current of 0.2 mA (50 s) and “power cycle” current of 0.5 mA or 2 mA (10 s) repeatedly during discharge, representing realistic values for the assembled validation electronics (Fig. 4c–e, S9 and S10†). For testing, a 25 cm<sup>2</sup> (5.3 mg cm<sup>-2</sup> MXene loading) device with five cells in series was used. The cell was charged at a constant voltage of 6 V for 27.5 min and then discharged at alternating current applying “standby” 0.2 mA for 50 s following a 10 s “power cycle” current of either 0.5 mA or 2 mA. Device discharge times significantly increase (106 min discharge with “standby” vs. 60 min at -0.5 mA) when “standby” current is introduced compared to when no “standby” current is used (Fig. S9 and S10†). We also observe that energy provided through multiple discharge cycles is consistent, when comparing the first power cycle with the 71st power cycle as shown in Fig. 4d–e and S9.† Consistency in energy provided during each discharge “power cycle” (Fig. S9†) as well as no device degradation at variable currents (Fig. S10†) guarantees that the peripheral hardware will function normally. Also, in Fig. S9† we can see that the energy delivered by the textile supercapacitors remains quite constant, which indicates a stable MXene/textile substrate interface. If the interface was broken, some small supercapacitors would have been disconnected from the system, which is not the case. This result shows that the variable current discharging testing matches the needs with respect to real-world wearable microelectronic

applications. In addition to wearables, the developed large-area flexible textile-based devices can be used for distributed energy storage in transportation, collapsible/inflatable tents, *etc.* They can also be combined with solar, triboelectric and other energy harvesting devices, providing full energy autonomy.<sup>37</sup>

**Integration with electronics.** While there's no shortage of flexible-form factor electronics suitable for e-textiles,<sup>5</sup> power for these devices still largely relies on traditional form factors like lithium-polymer (LiPo) and coin cell lithium batteries. As such, most e-textile systems do not use a flexible e-textile architecture that includes flexible energy storage. The MXene supercapacitor developed in this study fills the void, providing a textile-based energy storage solution that can power flexible electronics. We designed a simple peripheral electronics hardware system to validate our MXene textile supercapacitor, which includes the key components for any smart textile system – a sensor, a processor and a wireless transmitter/receiver for communication. Our supercapacitor is not only capable of powering a smart textile system but also compatible with other recent product developments highlighted in the literature.<sup>38–43</sup> The MXene-powered portion of the system (Fig. 5b, Device A) provides measurements from a temperature sensor (100 K thermistor) to a microcontroller (Arduino Pro Mini 3.3 V) which interfaces with a 2.4 GHz radio (NRF24L01+). It is important to note that the only power going to the microcontroller is from the supercapacitor, so the power consumption and the power output are identical. The microcontroller and firmware of

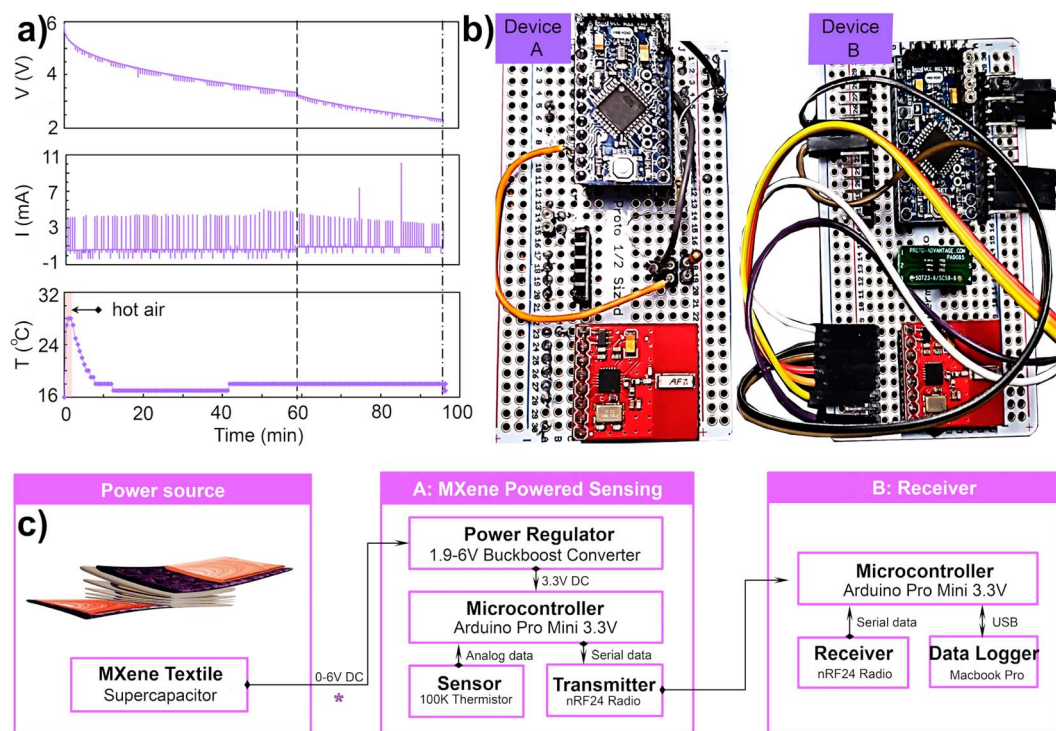


Fig. 5 (a) Discharge curves of devices being powered with a  $5 \times 5$  cm<sup>2</sup> 6 V textile-based supercapacitor with Ti<sub>3</sub>C<sub>2</sub>T<sub>x</sub> electrodes. (b) Image of the MXene powered sensing, computing, and transmitting device described in the hardware diagram. (c) System diagram for a basic computing hardware configuration that integrates a flexible textile-based supercapacitor as a power supply. Point \* denotes the layer between textile MXene and peripheral hardware, from which the discharge curve data in (a) was measured.



Device A were modified to reduce power consumption by removing onboard LEDs and utilizing a range of low-power open-source libraries to enhance sleep mode. However, in commercial e-textile devices,<sup>2</sup> custom designed hardware optimized for ultra-low power operation would further reduce the energy needs beyond our test setup, further increasing the runtime of the device. The system was programmed to take periodic measurements and transmit data to the receiver, while otherwise remaining in low power sleep mode (210 ms 'on' and 30 s 'standby'), drawing an average current in standby of 0.67 mA and peaking to 4.5 mA when on. The full system was constructed on a rigid board for testing with an MXene supercapacitor. While this board was composed of non-optimized components, the MXene textile supercapacitor was able to power the system and provide reliable wireless data output to a receiver for 96 min (Fig. 5a). Electronics were limited to operation between 6 and 2.1 V input due to onboard regulation on Device A, with input voltages below 3 V drawing considerably larger average currents, limiting the power accessible within the supercapacitor. Measurements using identical average current saw a time to discharge to 0 V time of 12 h 19 min (Fig. S11†), indicating that improved regulation could enable day-long use of the sensing device. Additionally, basic electrochemical performance of the textile device at various scan rates, various applied voltage windows and various discharge currents is provided in Fig. S6, S8 and S11.† Also, regarding the distribution of MXenes on yarn and electrochemical properties with different coating methods, Fig. S11† shows better performance with increased mass loading while Fig. 2 shows increased loading per deposition for drop casting. Fig. 5a shows voltage and current measurements of Device A gathered *via* a potentiostat (the schematics of the set-up for temperature measurements is shown in Fig. S12,† the discharge time into the temperature sensor system after supercapacitor precycling is shown in Fig. S13† (in Fig. S13† coulombic efficiency increases with cycling due to increase in charge density with subsequent cycles), and electrical circuit assembled for measurements using a potentiostat is shown in Fig. S14†), as well as the temperature data measured from Device A's onboard sensor. The simplified system diagrams in Fig. 5c illustrate the working principle of Devices A and B. Although the performance data in Fig. 5c were gathered from a freshly produced MXene sample, electrochemical testing signifies that the supercapacitor can operate even after 20 days of storage (Fig. S15†). An insignificant decrease in performance after storing for 20 days is due to minor water evaporation since manual vacuum sealing was used (Bonsenkitchen Vacuum Sealer Machine). On taking further steps towards commercialization of the device, such issues should not be a problem due to the use of a commercial vacuum sealing set-up. Dynamic bending of the device is demonstrated in ESI Video S1†.

**Charging protocols.** The textile MXene  $\text{Ti}_3\text{C}_2\text{T}_x$  supercapacitor having a  $25 \text{ cm}^2$  footprint area and  $5.3 \text{ mg cm}^{-2}$  loading with five cells vertically stacked in series was tested in a 6 V voltage window. Various charging methods were utilized to investigate the effect of charging protocols on the electrochemical performance of the supercapacitor. The techniques

include linear sweep voltammetry (LSV), galvanostatic cycling with potential limitations aka constant current (CC), constant voltage (CV), combination of CC with CV (as follows: CV, 10% CC, 30% CC, 50% CC, and 100% CC) and LSV. We set up all the charging procedures so that they lasted 27.5 min and reached a final voltage of 6 V. Longer charging minimized self-discharge due to ion redistribution within the large electrodes. To measure the effect that charging techniques had on the discharge behavior, galvanostatic discharge cycles were performed immediately after charging at a withdrawing current of 2.25 mA to 0 V, as shown in Fig. 4b (current and time was chosen based on a calibration curve provided in Fig. S4†). The LSV and 100% CC charging cycles underperformed compared to the others in terms of discharge time. The discharge cycles that performed the best were the cycles whose potentials had been held at 6 V using a 30 V/10 A DC Power Supply PS-3010DF. The charge cycle that spent the entire time at 6 V, performed the best, giving the longest discharge time (22 min 54 s at  $0.858 \text{ mA h capacity}$ ,  $20.602 \text{ mF cm}^{-2}$  capacitance and  $0.074 \text{ mW h cm}^{-2}$  energy density). Therefore, a constant voltage of 6 V was chosen as the charging protocol in the rest of the studies. The  $\text{Ti}_3\text{C}_2\text{T}_x$  MXene supercapacitor we used to power the peripheral electronics (Fig. S12 and Table S6†) was a five-cell device with a  $25 \text{ cm}^2$  footprint area and an MXene loading of  $24.2 \text{ mg cm}^{-2}$ . The textile supercapacitor was charged using a power supply (Dr meter 30 V/10 A DC Power Supply PS3010DF) while holding a constant voltage of 6 V for 60 minutes. There was no significant difference in device performance observed after 1 h and 2 h charging (Fig. S13†). For additional testing of the  $25 \text{ cm}^2$  footprint area device ( $5.3 \text{ mg cm}^{-2}$  MXene loading) (Fig. 4a and b), various commercially available unmodified microcontroller boards were powered (Fig. S3†). By substituting the microcontroller boards with sub-threshold processors or ultra-low power microcontrollers and reducing average current draws to under 0.1 mA, the MXene textile supercapacitor can be expected to provide considerably extended operation times.

## Conclusions

We have demonstrated that a textile-based energy storage device fabricated using a conductive additive-free  $\text{Ti}_3\text{C}_2\text{T}_x$  dispersion in water produces enough power to operate peripheral electronics hardware while remaining flexible and textile compliant. A  $\text{Ti}_3\text{C}_2\text{T}_x$  MXene textile supercapacitor device with a footprint area of  $25 \text{ cm}^2$  and MXene loading of  $24.2 \text{ mg cm}^{-2}$  reached an energy density of  $0.401 \text{ mW h cm}^{-2}$  at a power density of  $0.248 \text{ mW cm}^{-2}$  having a capacitance of  $146 \text{ mF cm}^{-2}$  at  $0.16 \text{ mA cm}^{-2}$  discharge current and a 6 V voltage window. The fully charged MXene supercapacitor was able to power unoptimized wireless electronics, transmitting temperature data every 30 seconds for 96 min, showing no degradation due to switching currents. A system designed and optimized for low power can be expected to operate considerably longer on a single  $25 \text{ cm}^2$  cell, potentially enabling a full day of use with multiple cells. The key to optimizing design is incorporating voltage regulation that accounts for the linear drop in the output voltage during discharge. Future work includes



development of ultra-low power electronics, while integrating our supercapacitor set-up as wearable garment patches, mechanical testing of MXene coatings on fabrics and yarns, and packaging optimization for increasing the shelf life.

## Author contributions

G. Dion supervised the textile aspects of the work. A. Danielescu supervised microelectronics application aspects of the work. Y. Gogotsi supervised the project. A. VahidMohammadi and R. J. Wang established protocols for electrochemical measurements. B. Greenspan and E. M. Gallo selected protocols and specific application goals for microelectronics assembly. T. Tabb assembled microelectronics and established its testing protocols. L. Bi took a lead on textile material selection and textile sample development. T. Hryhorchuk was responsible for  $\text{Ti}_3\text{C}_2\text{T}_x$  synthesis as well as preparation and testing of multicell supercapacitor samples. C. A. Inman developed strategy for high voltage multicell supercapacitor assembly and use of LiCl electrolyte for further voltage and energy increase. All authors discussed the results and reviewed the manuscript.

## Conflicts of interest

There are no conflicts to declare.

## Acknowledgements

We acknowledge Sol Schade and Simge Uzun for providing knitted single cell supercapacitor prototypes, Geetha Valurouthu for etching  $\text{Ti}_3\text{C}_2\text{T}_x$  used during testing on the initial samples, Adam Goad for sintering of the  $\text{Ti}_3\text{AlC}_2$  MAX phase and Christopher E. Shuck for performing XRD measurements and for multiple helpful discussions. This work was supported by Accenture. The electrochemical experiments were supported by the Fluid Interface Reactions, Structures and Transport (FIRST) Center, an Energy Frontier Research Center funded by the U.S. Department of Energy, Office of Science, Office of Basic Energy Sciences.

## Notes and references

- 1 K. Sakuma, *Flexible, Wearable, and Stretchable Electronics*, CRC Press, 2020.
- 2 C.-W. Kan and Y.-L. Lam, *Appl. Sci.*, 2021, **11**, 3914.
- 3 K. Hartman, *Make: Wearable Electronics: Design, Prototype, and Wear Your Own Interactive Garments*, Maker Media, Inc., 2014.
- 4 M. Kang and T.-W. Kim, *Appl. Sci.*, 2021, **11**, 6131.
- 5 N. A. Choudhry, L. Arnold, A. Rasheed, I. A. Khan and L. Wang, *Adv. Eng. Mater.*, 2021, **23**, 2100469.
- 6 M. Paeschke, U. Wollenberger, C. Köhler, T. Lisek, U. Schnakenberg and R. Hintsche, *Anal. Chim. Acta*, 1995, **305**, 126–136.
- 7 R. Tong, *Wearable Technology in Medicine and Health Care*, Academic Press, 2018.
- 8 A. P. Abidoye, N. A. Azeez, A. O. Adesina and K. K. Agbele, *J. Sens. Technol.*, 2011, **1**, 22–28.
- 9 C. G. Kanakry, *Sci. Transl. Med.*, 2020, **12**, eabb2779.
- 10 B. K. Deka, A. Hazarika, M.-J. Kwak, D. C. Kim, A. P. Jaiswal, H. G. Lee, J. Seo, C. Jeong, J.-H. Jang and Y.-B. Park, *Energy Storage Mater.*, 2021, **43**, 402–410.
- 11 G. Wu, Z. Yang, Z. Zhang, B. Ji, C. Hou, Y. Li, W. Jia, Q. Zhang and H. Wang, *Electrochim. Acta*, 2021, **395**, 139141.
- 12 S.-x. Yan, S.-h. Luo, Q. Wang, Y.-h. Zhang and X. Liu, *Composites, Part B*, 2021, **224**, 109246.
- 13 X. Zhang, H. Shi, L. Liu, C. Min, S. Liang, Z. Xu, Y. Xue, C. Hong and Z. Cai, *J. Colloid Interface Sci.*, 2022, **605**, 472–482.
- 14 W. Chen, M. Luo, K. Yang, C. Liu, D. Zhang and X. Zhou, *Chem. Eng. J.*, 2021, **423**, 130242.
- 15 L. Yang, F. Lin, F. Zabihi, S. Yang and M. Zhu, *Int. J. Biol. Macromol.*, 2021, **181**, 1063–1071.
- 16 H. Hwang, S. Byun, S. Yuk, S. Kim, S. H. Song and D. Lee, *Appl. Surf. Sci.*, 2021, **556**, 149710.
- 17 L. Qin, D. Yang, M. Zhang, T. Zhao, Z. Luo and Z.-Z. Yu, *J. Colloid Interface Sci.*, 2021, **589**, 264–274.
- 18 M. Naguib, M. Kurtoglu, V. Presser, J. Lu, J. Niu, M. Heon, L. Hultman, Y. Gogotsi and M. W. Barsoum, *Adv. Mater.*, 2011, **23**, 4207.
- 19 Z. Xiao, S. Ruan, L. B. Kong, W. Que, K. Zhou, Y. Liu and T. Zhang, *MXenes and MXenes-based composites*, Springer International Publishing, Cham, 2020.
- 20 B. Anasori and Y. G. Gogotsi, *2D Metal Carbides and Nitrides (MXenes)*, Springer, 2019.
- 21 A. VahidMohammadi, J. Rosen and Y. Gogotsi, *Science*, 2021, **372**, eabf1581.
- 22 C. J. Zhang, L. McKeon, M. P. Kremer, S.-H. Park, O. Ronan, A. Seral-Ascaso, S. Barwich, C. Ó. Coileáin, N. McEvoy and H. C. Nerl, *Nat. Commun.*, 2019, **10**, 1795.
- 23 S. Uzun, S. Seyedin, A. L. Stoltzfus, A. S. Levitt, M. Alhabeab, M. Anayee, C. J. Strobel, J. M. Razal, G. Dion and Y. Gogotsi, *Adv. Funct. Mater.*, 2019, **29**, 1905015.
- 24 K. Maleski, C. E. Shuck, A. T. Fafarman and Y. Gogotsi, *Adv. Opt. Mater.*, 2021, **9**, 2001563.
- 25 Q. Jiang, N. Kurra, M. Alhabeab, Y. Gogotsi and H. N. Alshareef, *Adv. Energy Mater.*, 2018, **8**, 1703043.
- 26 T. S. Mathis, K. Maleski, A. Goad, A. Sarycheva, M. Anayee, A. C. Foucher, K. Hantanasirisakul, C. E. Shuck, E. A. Stach and Y. Gogotsi, *ACS Nano*, 2021, **15**, 6420–6429.
- 27 M. R. Lukatskaya, S. Kota, Z. Lin, M.-Q. Zhao, N. Shpigel, M. D. Levi, J. Halim, P.-L. Taberna, M. W. Barsoum, P. Simon and Y. Gogotsi, *Nat. Energy*, 2017, **2**, 17105.
- 28 S. Seyedin, S. Uzun, A. Levitt, B. Anasori, G. Dion, Y. Gogotsi and J. M. Razal, *Adv. Funct. Mater.*, 2020, **30**, 1910504.
- 29 A. S. Levitt, M. Alhabeab, C. B. Hatter, A. Sarycheva, G. Dion and Y. Gogotsi, *J. Mater. Chem. A*, 2019, **7**, 269–277.
- 30 A. Levitt, D. Hegh, P. Phillips, S. Uzun, M. Anayee, J. M. Razal, Y. Gogotsi and G. Dion, *Mater. Today*, 2020, **34**, 17–29.
- 31 N. Driscoll, K. Maleski, A. G. Richardson, B. Murphy, B. Anasori, T. H. Lucas, Y. Gogotsi and F. Vitale, *J. Visualized Exp.*, 2020, e60741.

- 32 K. Maleski and M. Alhabeb, in *2D Metal Carbides and Nitrides (MXenes)*, ed. Y. Gogotsi and B. Anasori, Springer, Cham, 2019, pp. 69–87.
- 33 F. Shahzad, M. Alhabeb, C. B. Hatter, B. Anasori, S. Man Hong, C. M. Koo and Y. Gogotsi, *Science*, 2016, **353**, 1137–1140.
- 34 K. Maleski, C. E. Ren, M.-Q. Zhao, B. Anasori and Y. Gogotsi, *ACS Appl. Mater. Interfaces*, 2018, **10**, 24491–24498.
- 35 X. Wang, T. S. Mathis, Y. Sun, W.-Y. Tsai, N. Shpigel, H. Shao, D. Zhang, K. Hantanasirisakul, F. Malchik, N. Balke, D.-e. Jiang, P. Simon and Y. Gogotsi, *ACS Nano*, 2021, **15**, 15274–15284.
- 36 G. Wang, X. Lu, Y. Ling, T. Zhai, H. Wang, Y. Tong and Y. Li, *ACS Nano*, 2012, **6**, 10296–10302.
- 37 J. Song, B. Yang, W. Zeng, Z. Peng, S. Lin, J. Li and X. Tao, *Adv. Mater. Technol.*, 2018, **3**, 1800016.
- 38 R. Ma, Z. Chen, D. Zhao, X. Zhang, J. Zhuo, Y. Yin, X. Wang, G. Yang and F. Yi, *J. Mater. Chem. A*, 2021, **9**, 11501–11529.
- 39 G. Wu, Z. Ma, X. Wu, X. Zhu, Z. Man, W. Lu and J. Xu, *Angew. Chem.*, 2022, e202203765.
- 40 G. Wu, X. Wu, X. Zhu, J. Xu and N. Bao, *ACS Nano*, 2022, **16**, 10130–10155.
- 41 S. Sun, X. Zhu, X. Wu, M. Xu, Y. Hu, N. Bao and G. Wu, *J. Mater. Sci. Technol.*, 2023, **139**, 23–30.
- 42 M. Peng, L. Wang, L. Li, Z. Peng, X. Tang, T. Hu, K. Yuan and Y. Chen, *eScience*, 2021, **1**, 83–90.
- 43 G. Wu, S. Sun, X. Zhu, Z. Ma, Y. Zhang and N. Bao, *Angew. Chem., Int. Ed.*, 2022, **61**, e202115559.